Investigation of the Flow Structure Around a Rapidly Pitching Airfoil

Miguel R. Visbal* and J. S. Shang†
Air Force Wright Aeronautical Laboratories, Wright-Patterson Air Force Base, Ohio

A numerical study is presented for unsteady laminar flow past a NACA 0015 airfoil that is pitched, at a nominally constant rate, from zero incidence to a very high angle of attack. The flowfield simulation is obtained by solving the full two-dimensional compressible Navier-Stokes equations on a moving grid employing an implicit approximate-factorization algorithm. An evaluation of the accuracy of the computed solutions is presented, and the numerical results are shown to be of sufficient quality to merit physical interpretation. The highly unsteady flowfield structure is described and is found to be in qualitative agreement with available experimental observations. A discussion is provided for the effects of pitch rate and pitch axis location on the induced vortical structures and on the airfoil aerodynamic forces.

Nomenclature

c	= airfoil chord
C_L, C_D	= lift and drag coefficients
C_P	= pressure coefficient, $2(p-p_\infty)/\rho_\infty U_\infty^2$
M_∞	= freestream Mach number, $U_\infty/\sqrt{\gamma R T_\infty}$
n	= direction normal to airfoil surface
Re_c	= chord Reynolds number, $\rho_\infty U_\infty c/\mu_\infty$
u,v	= Cartesian velocity components in inertial frame of reference
U_∞	= freestream velocity
x,y,t	= Cartesian coordinates in inertial frame of reference and time
X,Y	= coordinate system attached to airfoil (Fig. 1)
X_0	= pitch axis location
α	= geometric angle of attack
α_{eff}	= effective angle of attack at airfoil leading edge
ξ,η,τ	= transformed coordinates
ν	= kinematic viscosity
Ω	= nondimensional pitch rate, $\Omega c/U_\infty$
ω	= vorticity, $\partial v/\partial x - \partial u/\partial y$
ω_F	= net vorticity flux at airfoil surface, $-\oint \nu \nabla \omega \cdot \mathbf{n}\, ds$
ω_F^+, ω_F^-	= positive (counterclockwise) and negative (clockwise) vorticity fluxes at airfoil surface

I. Introduction

THE understanding and potential utilization of unsteady separated flows constitute a challenging area of fluid mechanics. Within this broad flow category, one encounters the phenomenon of dynamic stall, a term loosely used to describe the complex physical events induced by the large-amplitude motion of aerodynamic bodies or lifting surfaces. Dynamic stall is of importance in various aerodynamic applications including aircraft maneuverability, helicopter rotors, and wind turbines. As the extensive reviews of McCroskey[1] and Carr[2] indicate, the majority of the research on dynamic stall has been devoted to the case of airfoils performing harmonic motions of moderate amplitude in a uniform incoming stream. For the cases when the airfoil reaches very high angles of attack, the generated flowfields are characterized by massive, unsteady separation and by large-scale vortical structures. Progress in this problem area is also complicated by the need to account for many interrelated flow parameters. In addition to the usual flowfield dependence on Mach number, Reynolds number, and airfoil shape, the effects of the form, rate, and amplitude of the forcing motion must be considered. Due to the complexity of these highly unsteady separated flows, the need for systematic computational and experimental studies is apparent. This current need constitutes the motivation for the present numerical investigation.

This paper presents a computational study of the unsteady laminar flow past an airfoil that is pitched at a constant rate to a very high angle of attack. The simple constant pitch rate motion represents the first logical step in a building-block approach, before more complex types of motion are considered. The constant pitch-up case should also permit the study of relevant dynamic stall phenomena, without introducing further complications associated with motion history effects. In addition, the large-amplitude constant pitch-rate case is of potential importance in future aircraft maneuverability.[3] Current interest in the present problem area is evidenced by the recent experimental investigations of Refs. 4–9 and the preliminary computational (viscous) studies of Visbal[10] and Wu et al.[11] The present work constitutes a more extensive and systematic study than those of Refs. 10 and 11.

Although the simulation of high Reynolds number (turbulent) flows is ultimately desired, the present computational results are limited to the case of low Reynolds number laminar flow. This constraint is imposed since a suitable model for transition and turbulence is not currently available for such a complex unsteady flow as the one under investigation. Nonetheless, the present laminar results are of value since they complement ongoing experimental efforts and provide clarification of important dynamic stall features and trends. This is particularly true in the high pitch-rate regime for which the energetic forcing motion is expected to temporarily dominate over some transition and turbulence effects. The favorable agreement found between predicted and experimental primary flow features confirms the previous hypothesis. Finally, two-dimensional results are of relevance since experimental flow visualizations[9] for a straight wing reveal a nearly two-dimensional flow structure (away from the wing tip) during the pitch-up motion.

The specific flow configuration considered is shown in Fig. 1. A NACA 0015 airfoil is pitched about a fixed axis at a constant rate from zero incidence to a maximum angle of attack of approximately 60 deg. The particular airfoil section selected has been used in the majority of pitch-up experimental stu-

Received June 23, 1987; revision received Sept. 21, 1988.

*Aerospace Engineer. Member AIAA.
†Technical Manager. Associate Fellow AIAA.

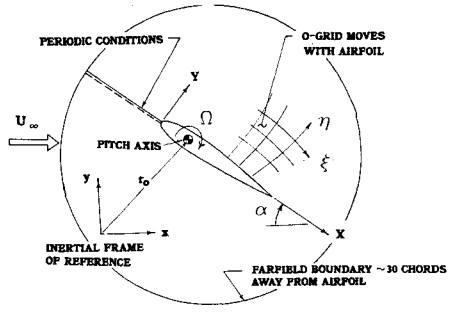

Fig. 1 Pitching airfoil configuration.

dies.[5-9] For the case of pure rotation, the similarity parameter associated with the airfoil motion is the nondimensional pitch rate $\Omega^+ = \Omega c/U_\infty$. This parameter arises in the nondimensionalization of the velocity boundary conditions on the airfoil surface, and it is simply the inverse of the Rossby number. Numerical results are obtained by solving the full compressible Navier-Stokes equations on a moving grid using an implicit approximate-factorization algorithm.[12] The main objectives of this study are summarized as follows: 1) description of the basic flowfield structure for the rapidly pitched airfoil, 2) parametric investigation of the effects of pitch-rate and pivot-axis location on the flow structure and aerodynamic loads, and 3) qualitative comparison of computed and experimental primary flow features.

II. Governing Equations and Boundary Conditions

For the case of external flow past a body in arbitrary motion, the governing equations can be formulated in an inertial frame or reference, and motion of the body can be provided for by means of a general time-dependent coordinate transformation. Introducing such a transformation [$\xi = \xi(x,y,t)$, $\eta = \eta(x,y,t)$, $\tau = t$], the full two-dimensional compressible Navier-Stokes equations may be expressed in the following strong-conservation form[13]:

$$\partial_\tau q + \partial_\xi E_1 + \partial_\eta E_2 = \partial_\xi (V_1 + V_2) + \partial_\eta (W_1 + W_2) \qquad (1)$$

where $q = J^{-1}[\rho, \rho u, \rho v, \rho e]$ is the vector of dependent variables. The form of the flux vectors appearing in Eq. (1) can be found in Ref. 13. Closure of this system of equations is provided by the perfect-gas law, Sutherland's viscosity formula, and the assumption of a constant Prandtl number.

In reference to the pitching airfoil configuration shown in Fig. 1, the boundary conditions are prescribed as follows. Along the inflow portion of the far-field boundary, free-stream conditions are given. First-order extrapolation ($\partial[\quad]/\partial x = 0$) is used for all flow variables on the outflow boundary. Along the O-grid cut, spatial periodicity is imposed in ξ by means of a five-station grid overlap. On the airfoil surface, the following isothermal, no slip condition is applied:

$$U = U_B,\ T_w = T_\infty,\ \partial p/\partial n = -\rho a_B \cdot \hat{n} \qquad (2)$$

where U_B and a_B denote, respectively, the velocity and acceleration on the airfoil surface that are known from the prescribed airfoil motion. For the nominally constant pitch-up motion considered in this paper, the following temporal variation, which avoids an infinite angular acceleration, is prescribed for Ω:

$$\Omega(t) = \Omega_0(1 - e^{-4.6t/t_0}),\ t \geq 0 \qquad (3)$$

where t_0 denotes the time taken by the airfoil to reach 99% of its final pitch rate Ω_0. The influence of t_0 on the computed flowfield had been previously investigated[10] and found to be limited to the early stages of the airfoil motion.

Table 1 Summary of pitching airfoil computations (NACA 0015 airfoil, $M_\infty = 0.2$, $Re_c = 10^4$)[a]

Case	Ω_0^+	t_0^+	X_0/c
1	0.1	0.5	0.25
2	0.1	0.5	0.75
3	0.2	0.5	0.0
4	0.2	0.5	0.25
5	0.2	0.5	0.75
6	0.4	1.0	0.0
7	0.4	1.0	0.25
8	0.4	1.0	0.5
9	0.4	1.0	0.75
10	0.6	1.0	0.0
11	0.6	1.0	0.25
12	0.6	1.0	0.75

[a] Ω_0^+ = nondimensional pitch rate, $\Omega_0\, c/U_\infty$; t_0^+ = nondimensional acceleration time, $t_0 U_\infty/c$ [Eq. (3)]; X_0/c = pivot axis location measured from airfoil leading edge.

Finally, the formulation of the problem is completed by imposing as an initial condition the computed flow at 0 deg angle of attack.

III. Numerical Procedure

The time-dependent coordinate transformation (i.e., moving grid) required in the present flow simulation is implemented using a "rigid" grid attached to the airfoil.[13] This approach is employed since it eliminates the need for multiple-grid generation. Once an initial grid is constructed, the physical coordinates (x,y) and grid speeds (x_τ, y_τ) can be easily computed from the prescribed airfoil motion.

Nearly orthogonal boundary-fitted 0-grids are generated about the airfoil employing the elliptic technique of Ref. 14. Three different grid sizes are considered (113 × 51, 203 × 101, and 304 × 123). The medium grid, selected for the majority of the calculations, extends approximately 30 chords away from the airfoil and has minimum spacings of $0.00075c$ and $0.00005c$ in the ξ and η directions, respectively.

The governing equations are numerically solved employing the implicit approximate-factorization algorithm of Beam and Warming.[12] This scheme is formulated using three-point backward time differencing and second-order centered approximations for all spatial derivatives. In order to control numerical stability, both explicit and implicit smoothing terms are added to the basic algorithm. A fully vectorized Navier-Stokes solver that employs the above scheme has been developed and successfully validated for a variety of both steady and unsteady flow problems.[10,15,16]

IV. Results and Discussion

Calculations were performed for the flowfield configuration depicted in Fig. 1. A NACA 0015 airfoil was pitched about a fixed axis from zero incidence to a maximum angle of attack of approximately 60 deg with an angular velocity of the form given by Eq. (3). The freestream Mach number and chord Reynolds number were 0.2 and 10^4, respectively. A summary of all cases computed is provided in Table 1. The discussion of the present results is divided into the following major areas: 1) evaluation of the accuracy of the computed results, 2) description of the basic flowfield structure, and 3) parametric effects of pitch rate and pivot-axis location.

Evaluation of the Accuracy of the Computed Solutions

Before proceeding to make any observations pertaining to the physical aspects of the flow, estimates of the accuracy of the computed solutions must be provided. In the present calculations, numerical uncertainties were mainly associated with time discretization (i.e., time step value), spatial resolution,

and numerical damping terms. Other sources of error (e.g., far-field boundary location and implementation of implicit boundary conditions) were previously investigated[10] for an unsteady separated flow and found to be of less significance.

The effect of the time step value on the computed pitching airfoil flow was documented in Ref. 10 for the case of $\Omega_0^+ = 0.2$ (case 4, Table 1). It was concluded in that study that a numerical solution effectively independent of time step was achieved if $\Delta t U_\infty / c \leq 0.001$. Therefore, this time step value was specified in all the present calculations.

The sensitivity of the computed flowfield to spatial resolution was evaluated for the case when $\Omega_0^+ = 0.6$ (case 11, Table 1). Calculations were performed using the three different grid systems, previously discussed in Sec. III. Although further grid refinements are desirable, the finest (304×123) grid employed was the largest one possible given the available computer resources (Cray XMP/12). The effect of the grid size on the predicted lift and drag coefficients is shown in Fig. 2. The maximum difference in C_L between the fine and the medium grid was approximately 3.5%, and it was less then 1% for $\alpha \leq 40$ deg. Figure 3 is a plot of isovorticity contours obtained with the three different grid systems. It can be observed that the first grid refinement produced significant changes in the computed solution. However, after the second mesh refinement, the discrepancies were considerably reduced and did not alter the primary vortical structures in the vicinity of the airfoil. Therefore, the medium grid was considered suitable for the present study. Finally, the sensitivity of the solution to numerical smoothing was also evaluated for the medium grid. It was found[17] that increasing the damping coefficient by a factor of two produced only small changes in the computed vorticity field without altering its primary structure. The present limited accuracy study seems to indicate that the computed results are of sufficient quality to merit further physical interpretation.

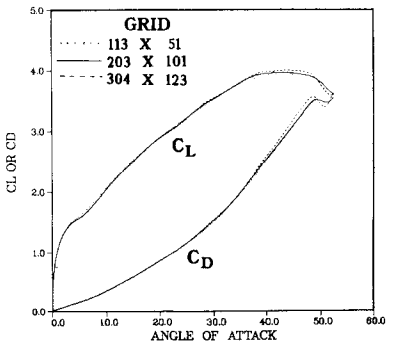

Fig. 2 Effect of spatial resolution on computed lift and drag coefficients (case 11).

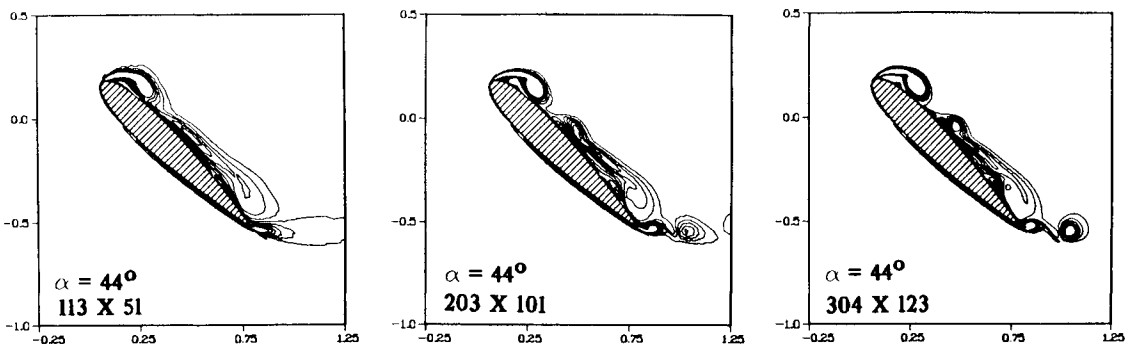

Fig. 3 Effect of spatial resolution on vorticity field (case 11).

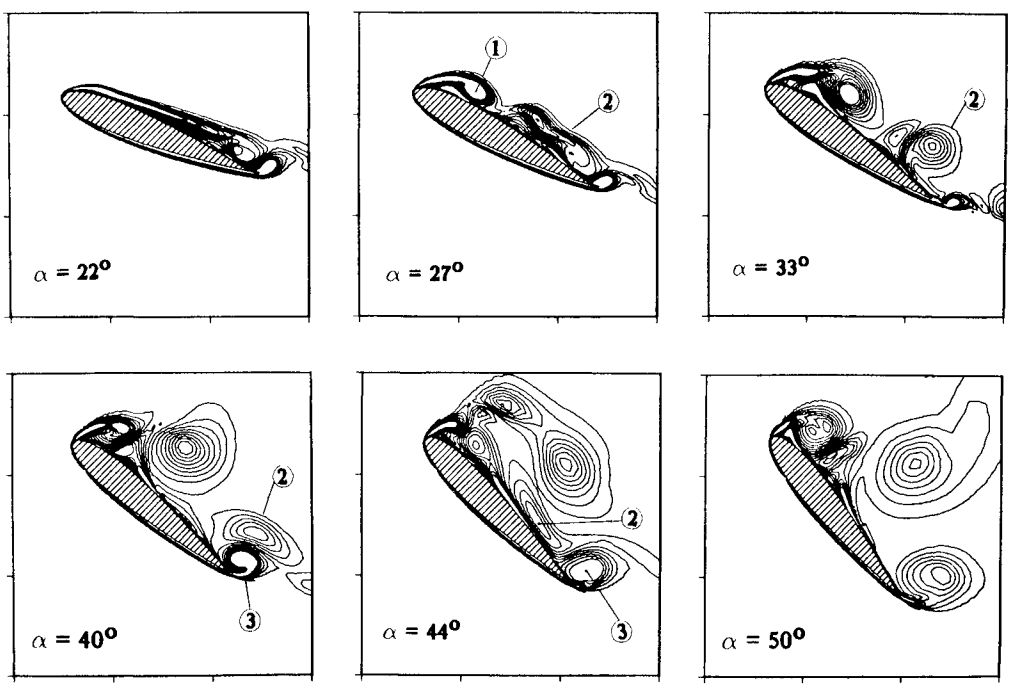

Fig. 4 Evolution of vorticity field (case 4): 1) leading-edge vortex, 2) shear layer vortex, 3) trailing-edge vortex.

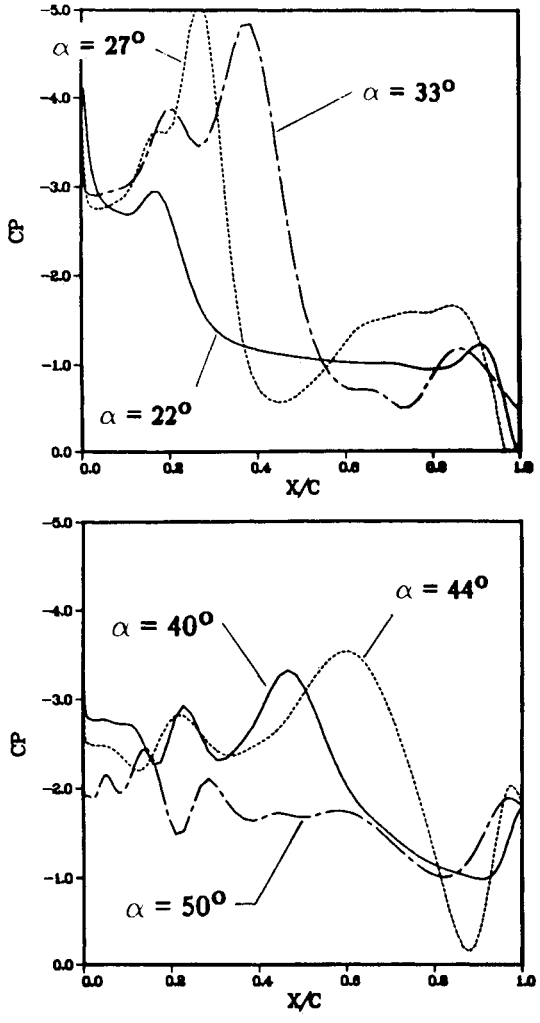

Fig. 5 Computed airfoil surface pressure distributions (case 4).

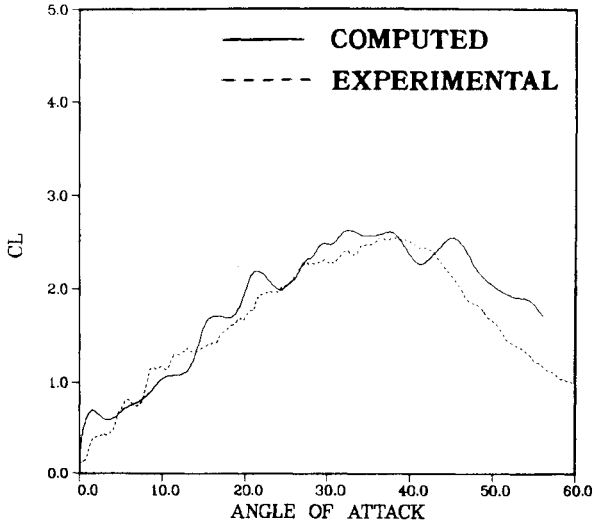

Fig. 6 Comparison of computed and experimental lift coefficients ($\Omega_0^+ = 0.2$, $X_0/c = 0.25$, $Re_c = 45{,}000$).

Basic Flowfield Structure

This section presents a description of the most important unsteady features of the flow past a pitching airfoil. This is done in order to set the stage for the subsequent discussion of parametric effects. The flowfield evolution for the case when $\Omega_0^+ = 0.2$ (case 4, Table 1) is provided by means of isovorticity contours (Fig. 4) and surface pressure distributions (Fig. 5). From these figures as well as from a computer-generated color movie, the following sequence of flow events is observed.

At zero incidence, the flow is symmetric and displays a small trailing-edge separation region. As the pitching motion begins, the flow becomes fully attached along the airfoil lower surface, while on the upper surface the separation point moves upstream (Fig. 4a). The near-wake experiences significant curvature and after a short time reorganizes itself into a series of discrete vortices (Fig. 4a). Counterclockwise (positive) vortices are shed from the lower-surface boundary layer into the wake, in accordance with the corresponding increase in the airfoil clockwise circulation and lift. With the continuous increase in airfoil incidence, the upper-surface separation region eventually reaches the leading-edge area. Subsequently, the separated shear layer reattaches, dividing the upper-surface flow into two distinguishable vortical structures denoted as the leading-edge or dynamic stall vortex and the shear layer vortex (Fig. 4b). The latter is in itself composed of two substructures that rotate about each other and later amalgamate to form a single vortex (Fig. 4c). The leading-edge vortex grows in size, and its center is displaced downstream (Figs. 4b–4d), as also evidenced by the pressure distribution (Fig. 5). The leading-edge vortex detaches when its center is approximately at the midchord location. By this time, a well-defined and rapidly growing counterclockwise vortex is observed to remain attached to the trailing edge (Fig. 4e). The shear layer vortex, which had begun to be convected downstream (Fig. 4d), is brought back and impinges on the airfoil surface due to the combined influence of the leading and trailing-edge vortices (Fig. 4e). In a very complex interaction, which involves dramatic rotational effects, the leading-edge vortex and the shear layer vortex combine to form a larger vortical structure (Fig. 4f). This structure is then convected along a path nearly normal to the airfoil chord due to the blockage effect of the trailing-edge vortex.

The basic flow structure previously described is in qualitative agreement with experimental flow visualizations[6] obtained for $Re_c = 4.5 \times 10.^4$ In order to permit a more direct comparison with the experiments, the case when $\Omega_0^+ = 0.2$ and $X_0/c = 0.25$ (case 4, Table 1) was recomputed using a chord Reynolds number of 45,000, while still retaining the assumption of laminar flow. A comparison of the computed and experimental[7] lift coefficient histories is shown in Fig. 6. The agreement is reasonable, despite the assumption of laminar flow employed in the calculation. In particular, the maximum lift value and the angle of attack at which it occurs are in close agreement. A comparison of the computed streaklines with the experimental[6] smoke visualizations are primarily characterized by a well-defined recirculation region on the airfoil leeward side, which corresponds to the dynamic stall vortex. Figure 7 also indicates reasonable agreement between the computation and the experiment regarding the size and location of the dynamic stall vortex.

Effects of Pitch Rate and Pitch-Axis Location

The dependence of the flowfield structure on the pitch rate and the pivot location was investigated. As Table 1 indicates, the nondimensional pitch rate was varied over the range 0.1–0.6 and four different axis locations were considered ($X_0/c = 0$, 0.25, 0.5, and 0.75). The influence of pitch rate and axis location on the flow is discussed in terms of how these parameters affect the observed vortical structure and the airfoil aerodynamic loads.

Effect of Ω_0^+ and X_0/c on the Vortical Structure

Figures 8 and 9 show the vorticity field at three angles of attack for four different cases. Based on these figures and similar ones,[17] the following major observations can be drawn pertaining to the qualitative aspects of the vortical structure:

1) Over the range of Ω_0^+ and X_0/c considered, the flow was qualitatively characterized by the same primary features, which included: upstream propagation of the trailing-edge separation region on the airfoil upper surface and formation

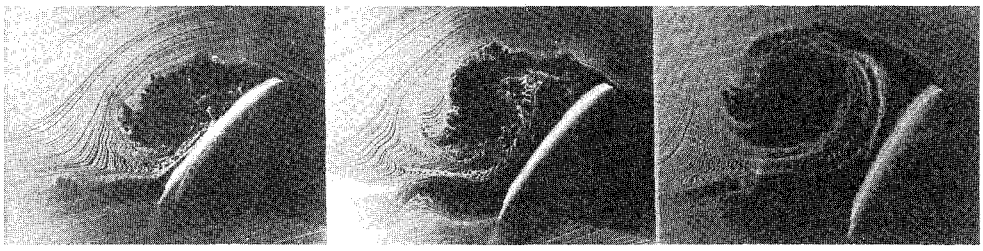

a) Experimental smoke visualization

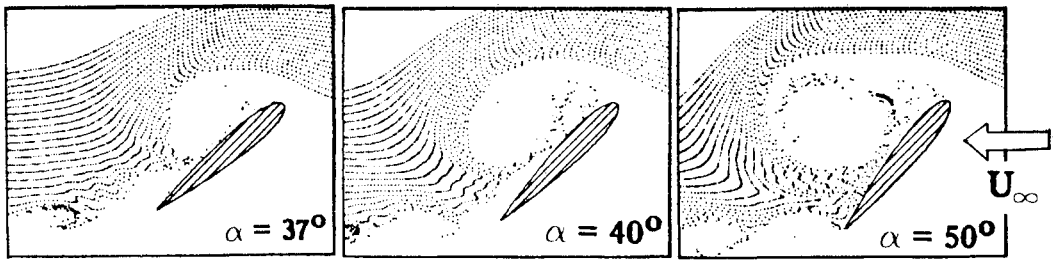

b) Computed streaklines

Fig. 7 Comparison of computed and experimental flow visualizations ($\Omega_0^+ = 0.2$, $X_0/c = 0.25$, $Re_c = 45{,}000$).

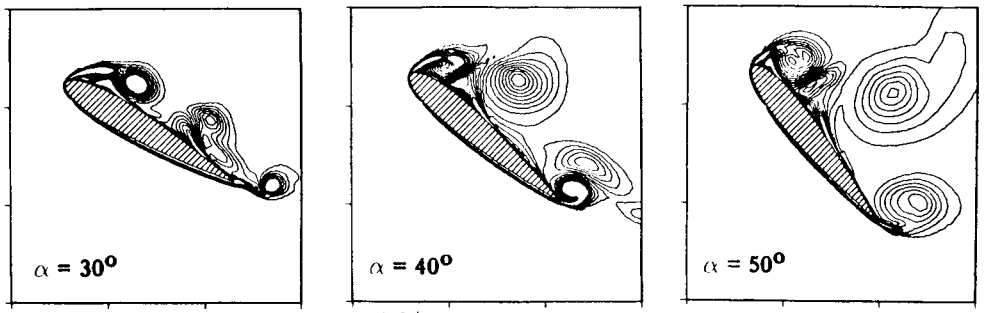

a) $\Omega_0^+ = 0.2$, $X_0/c = 0.25$

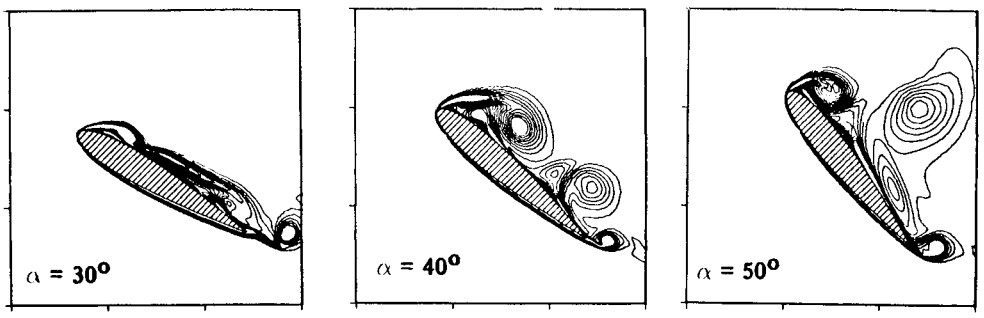

b) $\Omega_0^+ = 0.2$, $X_0/c = 0.75$

Fig. 8 Evolution of vorticity field for cases 4 and 5.

of a leading-edge vortex and a shear layer vortex, as well as their complex interaction. However, the quantitative characterization of these basic features (e.g., timing, vortex strength, etc.) showed a strong dependence on both the pitch rate and the axis location.

2) For a fixed-pitch axis location downstream of the leading edge, increasing the pitch rate resulted in the formation of the leading-edge vortex at a higher angle of attack (Figs. 8 and 9), in accordance with experimental observations.[6]

3) For a fixed value of Ω_0^+, displacing the pitch axis downstream delayed the leading-edge vortex formation (Figs. 8 and 9). This behavior was found to be related to an "effective" angle of attack (α_{eff}), which can be defined by subtracting from U_∞ the pitch motion induced airfoil velocity at the leading edge $U_{B_{\text{L.E.}}} = \Omega \times (r_{\text{L.E.}} - r_0)$. The correlation of the leading-edge vortex formation with α_{eff} is shown in Fig. 10 for cases 6 and 9 (Table 1). At the same effective incidence ($\alpha_{\text{eff}} = 30$ deg), the dynamic stall vortex is observed to be in both cases at the same stage of development, despite the large difference in geometric angle of attack. Since the magnitude of $U_{B_{\text{L.E.}}}$ is $\Omega_0^+ \mid X_0/c \mid$, displacing the pitch axis downstream results in a redution of α_{eff} (for a fixed Ω_0^+ and at a given α) and in an additional delay of stall. Furthermore, the changes produced by a given axis shift will increase proportionally with the value of pitch rate itself.

After the above remarks on the qualitative features of the vorticity field, we now discuss a few of its quantitative aspects. Figure 11 shows the minimum surface pressure level (or "suction peak") induced by the leading-edge vortex, for different pitch rates and pitch-axis locations. These high suction values can be interpreted only as an *approximate* measure of the leading-edge vortex strength. As Fig. 11 indicates, the magnitude of the suction peak is a function of both pitch rate and axis location. However, the influence of the pivot location on

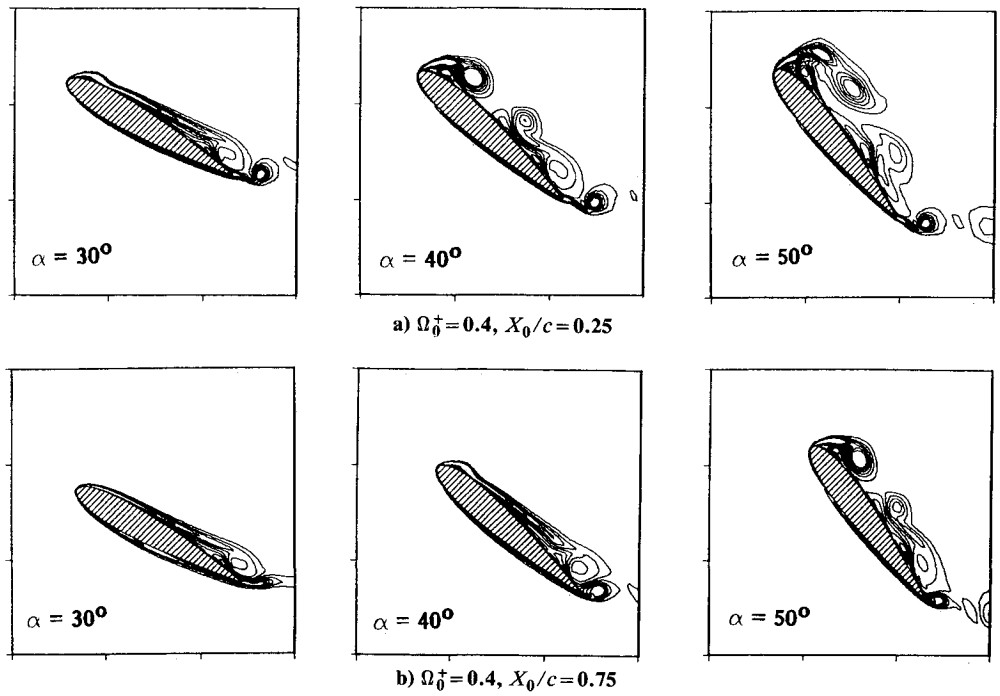

a) $\Omega_0^+ = 0.4$, $X_0/c = 0.25$

b) $\Omega_0^+ = 0.4$, $X_0/c = 0.75$

Fig. 9 Evolution of vorticity field for cases 7 and 9.

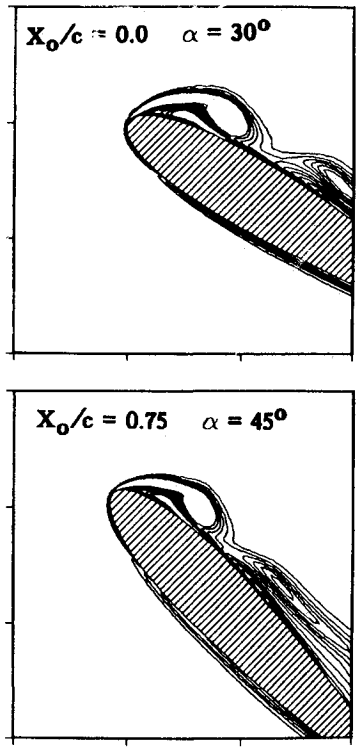

Fig. 10 Correlation of the leading-edge vortex formation with the effective angle of attack ($\alpha_{eff} = 30$ deg, cases 6 and 9).

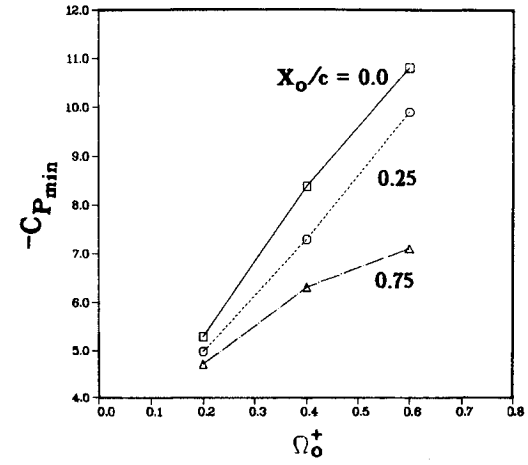

Fig. 11 Effect on Ω_0^+ and X_0/c on the vortex-induced suction peak.

Cp_{min} is not very significant for $\Omega_0^+ < 0.2$. Increasing Ω_0^+ (with constant X_0/c) or displacing the axis upstream (for fixed Ω_0^+) result in a stronger suction peak.

Since the vorticity present in the flowfield is introduced at the airfoil surface by diffusion, it is of interest to document how the net vorticity flux at the wall varies as a function of pitch rate and axis position. As Fig. 12a indicates, the net flux of vorticity ω_F is only significant during the period of angular acceleration and becomes negligible once a constant pitch rate is reached. The net vorticity flux increases with Ω_0^+ but is independent of the pitch-axis loction. This behavior of ω_F is consistent with the law of vorticity conservation as explained in Ref. 19 for the case of incompressible flow. The counterclockwise vorticity flux ω_F^+ and the clockwise vorticity flux ω_F^- are shown separately in Fig. 12b. It can be seen that ω_F^+ and ω_F^- are dependent on both pitch rate and axis position. For instance, by increasing Ω_0^+ or displacing the axis upstream, more clockwise vorticity is introduced into the flow. This observed variation of ω_F^- as a function of Ω_0^+ and X_0/c correlates well with the strength of the vortex-induced suction peak previously discussed (Fig. 11).

Effect of Ω_0^+ and X_0/c on the Aerodynamic Loads

The variation of the maximum lift coefficient $C_{L_{max}}$ as a function of pitch rate and pivot-axis location is shown in Fig. 13. Some experimental results from Refs. 7, 8, and 20 are also included for comparison. The maximum lift is dependent on both pitch rate and axis position, with the influence of pivot location being quite significant for $\Omega_0^+ > 0.2$. In all cases, it is found that for a fixed Ω_0^+ the downstream displacement of the pitch axis results in a reduction in lift. It is interesting to recall from the previous section that the aft motion of the axis resulted also in a delay of the leading-edge vortex formation (Figs. 8 and 9). Therefore, one cannot assume that further delays in the leading-edge vortex formation will always be accompanied by a higher airfoil lift.

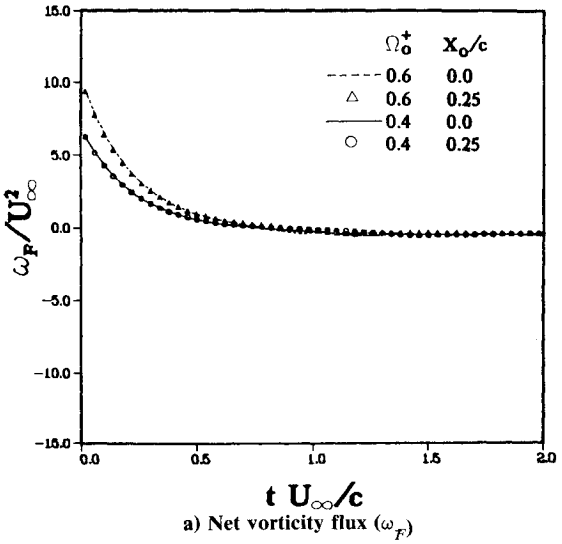

a) Net vorticity flux (ω_F)

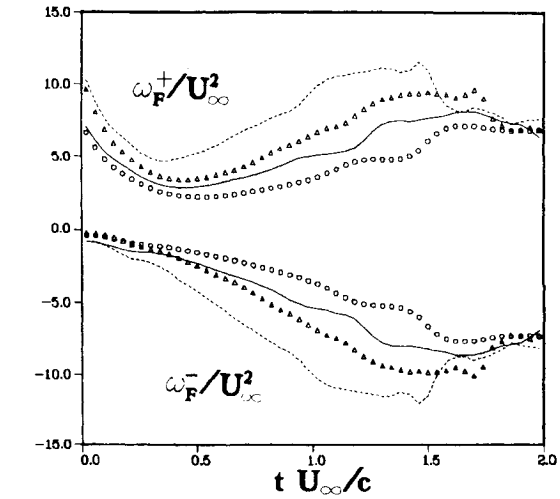

b) Positive (ω_F^+) and negative (ω_F^-) vorticity fluxes

Fig. 12 Effect of Ω_0^+ and X_0/c on the airfoil surface vorticity flux.

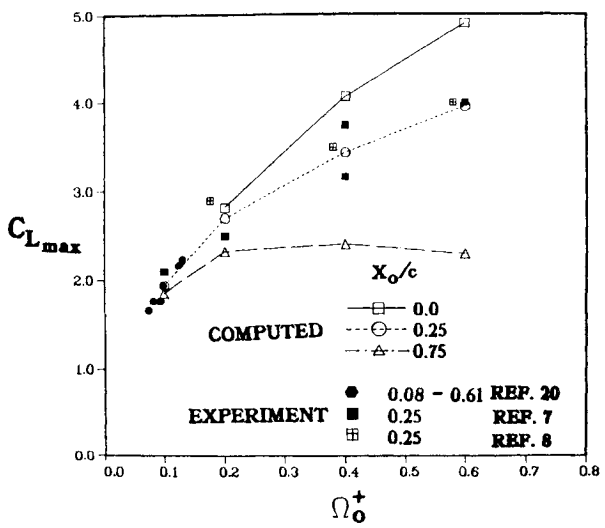

Fig. 13 Effect on Ω_0^+ and X_0/c on the maximum lift coefficient.

The dependence of $C_{L_{max}}$ on the pitch rate also can be clearly seen in Fig. 13. For $X_0/c=0$ and 0.25, the maximum lift coefficient is approximately proportional to $\sqrt{\Omega_0^+}$ over the range of pitch rates considered. For $X_0/c=0.75$, $C_{L_{max}}$ increases with pitch rate for $\Omega_0^+ \leq 0.2$, but then remains nearly

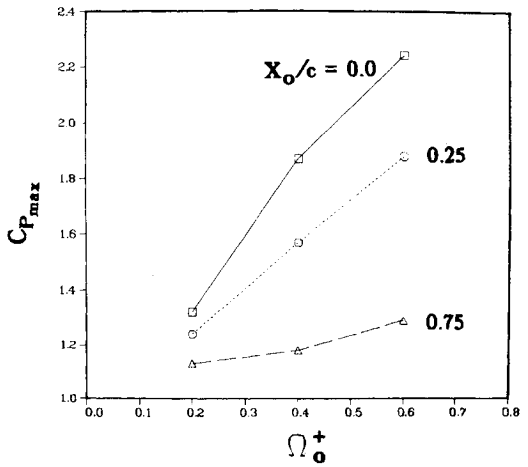

Fig. 14 Effect of Ω_0^+ and X_0/c on the maximum lower surface pressure coefficient.

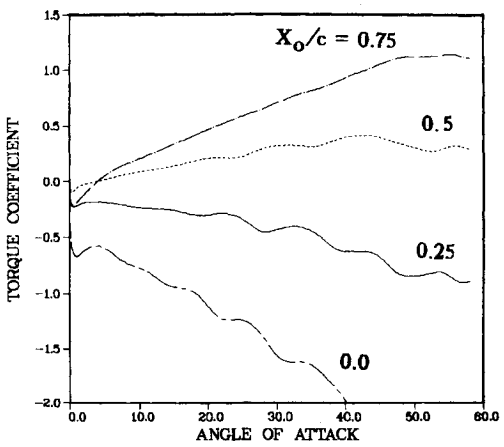

Fig. 15 Effect of pivot location on the torque coefficient ($\Omega_0^+=0.4$).

constant over the range $0.2 \leq \Omega_0^+ \leq 0.4$, and eventually begins to decrease when $\Omega_0^+ \geq 0.4$.

A precise explanation of the large aerodynamic loads experienced by the airfoil and of their dependence on the pitch rate and axis location constitutes a difficult problem. In the theoretical work of Wu,[19] it is shown that the force exerted by the fluid on the airfoil is the result of two contributing terms. The first term is proportional to the time rate of change of the total first moment of vorticity, while the second term is an inertia force associated with the mass of fluid displaced by the airfoil. For the case of constant rotation rate about a fixed axis, the second term is proportional to $(\Omega_0^+)^2(A/c^2)\,(r_c/c)$ where r_c/c denotes the distance from the pitch axis to the centroid of the airfoil of area A. This contribution, which has the form of a centrifugal force, is not significant for the pitch rates and pitch axis locations considered in the present investigation ($\Omega_0^+<1$, $A/c^2<1, r_c/c<1$). The large aerodynamic loads observed are therefore the result of the time rate of change of the first moment of vorticity. On a qualitative basis, vorticity-moment arguments suggest that the large transient forces are caused by substantial amounts of counterclockwise vorticity being shed from the lower surface boundary layer into the wake, while the corresponding clockwise vorticity (which must be present according to vorticity conservation) temporarily remains in the vicinity of the airfoil due to the formation of the leading-edge vortex. This behavior is the key feature observed in the present computations, as well as in experimental flow visualization.[6,18]

To conclude this section, a few remarks are included regarding the effect of the pitch-axis location on the aerodynamic

loads. The position of the pitch axis determines how much of the airfoil is moving against the incoming flow. This is seen more clearly for the extreme cases when $X_0/c \leq 0$ and ≥ 1.0. When the pitch axis is at the leading edge, the airfoil moves as a whole against the incoming flow. On the other hand, when the pivot is at the trailing edge, the airfoil is retreating. Displacing the pivot axis upstream therefore should result in higher pressures on the airfoil windward surface. This is shown in Fig. 14 in terms of the maximum stagnation pressure coefficient Cp_{max} as a function of Ω_0^+ and X_0/c. In addition, for a fixed Ω_0^+, the pitch-axis position determines the relative velocities at the airfoil leading and trailing edges. Moving the axis upstream increases α_{eff} as well as the relative velocity at the trailing edge. As the pitch axis is displaced forward, the increase in α_{eff} and Cp_{max} (Fig. 14) result in higher pressure gradients along the airfoil surface near the leading edge. This increase in the pressure gradient causes a higher vorticity flux (see ω_F^-, Fig. 12b) and a higher lift (Fig. 13), since also more counterclockwise vorticity can be shed at the trailing edge from the lower surface boundary layer into the wake.

Finally, the location of the pitch axis determines whether the airfoil actually imparts or extracts energy from the incoming flow. This is illustrated in Fig. 15, which shows the moment coefficient about the pivot axis, that is to say, the torque required to maintain the prescribed constant pitch-rate motion. It can be seen that, for $X_0/c = 0.5$ and 0.75, the torque exerted by the fluid on the airfoil is in the direction of rotation and, consequently, the airfoil extracts energy from the surrounding stream.

V. Concluding Remarks

A numerical study was conducted for the case of laminar flow around a NACA 0015 airfoil that pitches at a constant rate to a very high angle of attack. The highly unsteady flow structure was found to be characterized by 1) upstream propagation of separation from the trailing edge, 2) shedding of counterclockwise vortices into the wake, 3) the formation of a leading-edge vortex and a shear layer vortex on the airfoil leeward side, and 4) the complex interaction of these vortices as they are being shed. The basic flowfield structure for high pitch rates was shown to be in qualitative agreement with experimental observations, in spite of the assumption of laminar flow.

The dependence of the flowfield on the pitch rate and the pivot axis location was investigated. Over the range of Ω_0^+ and X_0/c considered, the flow displayed the same primary features or flow events. However, the quantitative characterization of these features showed a strong dependence on both the pitch rate and the axis position. For a given pitch rate, the downstream displacement of the pivot axis resulted in a delay in the dynamic stall vortex formation and in a reduction in the airfoil aerodynamic forces. For a given axis location downstream of the leading edge, increasing the pitch rate caused the dynamic stall vortex to form at a higher incidence. The maximum lift may either increase or decrease with increasing pitch rate, depending upon the axis placement.

Acknowledgment

The authors are grateful to Maj. J. Walker of Frank J. Seiler Research Laboratory for his assistance in providing some of the experimental data.

References

[1]McCroskey, W. J., "Unsteady Airfoils," *Annual Review of Fluid Mechanics,* Vol. 14, 1982, pp. 285–311.

[2]Carr, L. W., "Progress in Analyses and Prediction of Dynamic Stall," *Journal of Aircraft*, Vol. 25, Jan. 1988, pp. 6–17.

[3]Lang, J. D. and Frances, M. S., "Unsteady Aerodynamics and Dynamic Aircraft Maneuverability," AGARD CP-386, Nov. 1985.

[4]Francis, M. S. and Keesee, J. E., "Airfoil Dynamic Stall Performance with Large-Amplitude Motions," *AIAA Journal,* Vol. 23, Nov. 1985, pp. 1653–1659.

[5]Jumper, E. J., Shreck, S. J., and Dimmick, R. L., "Lift-Curve Characteristics for an Airfoil Pitching at Constant Rate," *Journal of Aircraft,* Vol. 24, Oct. 1987, p.. 680–685.

[6]Helin, H. E. and Walker, J. M., "Interrelated Effects of Pitch Rate and Pivot Point on Airfoil Dynamic Stall," AIAA Paper 85-0130, Jan. 1985.

[7]Walker, J., Helin, H., and Chou, D., "Unsteady Surface Pressure Measurements on a Pitching Airfoil," AIAA Paper 85-0532, March 1985.

[8]Strickland, J. H. and Graham, G. M., "Force Coefficients for a NACA 0015 Airfoil Undergoing Constant Pitch Rate Motions," *AIAA Journal,* Vol. 25, April 1987, pp. 622–624.

[9]Robinson, M., Helin, H., Gilliam, F., Russell, J., and Walker, J. "Visualization of Three-Dimensional Forced Unsteady Separated Flow," AIAA Paper 86-1066, May 1986.

[10]Visbal, M. R., "Evaluation of an Implicit Navier-Stokes Solver for Some Unsteady Separated Flows," AIAA Paper 86-1053, May 1986.

[11]Wu, J. C., Wang, C. M., and Tuncer, I. H., "Unsteady Aerodynamics of Rapidly Pitched Airfoils," AIAA Paper 86-1105, 1985.

[12]Beam, R. and Warming, R., "An Implicit Factored Scheme for the Compressible Navier-Stokes Equations," *AIAA Journal,* Vol. 16, April 1978, pp. 393–402.

[13]Steger, J., "Implicit Finite-Difference Simulation of Flow About Arbitrary Two-Dimensional Geometries," *AIAA Journal*, Vol. 16, July 1978, pp 679–686.

[14]Visbal, M. and Knight, D., "Generation of Orthogonal and Nearly Orthogonal Coordinates with Grid Control Near Boundaries," *AIAA Journal,* Vol. 20, March 1982, pp. 305–306.

[15]Visbal, M. and Knight, D., "The Baldwin-Lomax Turbulent Model for Two-Dimensional Shock-Wave/Boundary-Layer Interactions," *AIAA Journal,* Vol. 22, July 1984, pp. 921–928.

[16]Visbal, M. R. and Shang, J. S., "Comparative Study Between Two Navier-Stokes Algorithms for Transonic Airfoils," *AIAA Journal,* Vol. 24, April 1986, pp. 599–606.

[17]Visbal, M. and Shang, J., "Numerical Investigation of the Flow Structure Around a Rapidly Pitching Airfoil," AIAA Paper 87-1424, June 1987.

[18]Walker, J. M., Helin, H. E., and Strickland, J. H., "An Experimental Investigation of an Airfoil Undergoing Large-Amplitude Pitching Motions," *AIAA Journal,* Vol. 23, Aug. 1985, pp. 1141–1142.

[19]Wu, J. C., "Theory for Aerodynamic Force and Moment in Viscous Flows," *AIAA Journal,* Vol. 19, April 1981, pp. 432–441.

[20]Dimmick, R. L., "Pitch-Location Effects on Dynamic Stall," M. S. Thesis, Air Force Institute of Technology, Wright-Patterson AFB, OH, Rept. AFIT/GAE/AA 85 D-4, Dec. 1985.